minerals

MDPI

Article

Flotation of a Copper Oxide–Sulfide Ore Using NaHS-Assisted Sulfidization and 2,5-Dimercapto-1,3,4-Thiadiazole (DMTD) as a Collector: Experimental and DFT Insights

Isa Nozari [1], Asghar Azizi [1,*], Hamed Dehghani [2], Deniz Karataş [3] and Ahmad Hassanzadeh [4,5,*]

[1] Faculty of Mining, Petroleum & Geophysics Engineering, Shahrood University of Technology, Shahrood 3619995161, Iran; isa.nozari@shahroodut.ac.ir
[2] Department of Mining & Metallurgical Engineering, Amirkabir University of Technology, Tehran 1591634311, Iran; hameddehghani@aut.ac.ir
[3] Soma Vocational School, Manisa Celal Bayar University, Manisa 45500, Turkey; deniz.karatas@cbu.edu.tr
[4] Maelgwyn Mineral Services Ltd., Ty Maelgwyn, 1A Gower Street, Cathays, Cardiff CF24 4PA, UK
[5] Behraz Energy Ashkan Ltd., Jomhouri Boulevard, Kerman 7618868366, Iran
* Correspondence: aazizi@shahroodut.ac.ir or azizi.asghar22@yahoo.com (A.A.); ahassanzadeh@maelgwyn.com (A.H.)

Abstract

Flotation of mixed copper oxide–sulfide ores remains challenging due to low natural floatability of oxide minerals and complex interplay between sulfidization and collector adsorption. This study investigated the combined effect of NaHS-assisted sulfidization and 2,5-dimercapto-1,3,4-thiadiazole (DMTD), an azole-based collector, in terms of enhancing copper recovery from a mixed oxide–sulfide ore. The effects of pulp pH, DMTD, NaHS, and sodium metasilicate dosages, together with pulp solid concentration, were evaluated using response surface methodology. The quadratic model showed high predictive capability (R^2 = 0.9361), identifying NaHS dosage as the most influential factor. Optimum operating conditions (pH 9.50, DMTD 200 g/t, NaHS 750 g/t, sodium metasilicate 500 g/t, and 25% solids) yielded 64.03% copper recovery. Compared with the plant collector (PAX, Potassium Amyl Xanthate), DMTD increased recovery by 12.6% for highly oxidized ore while producing a higher concentrate grade. Density Functional Theory (DFT) calculations provided molecular insights into the experimental observations, confirming DMTD's high affinity for sulfidized surfaces. Hybrid solvation models revealed greater thermodynamic stability (ΔE_{ads} = −6.74 eV) than PAX due to hydrogen bonding with explicit water molecules, while the smaller HOMO–LUMO gap (ΔE_{gap} = 0.86 eV) supported its superior electron transfer capability and reactivity. These findings demonstrate that NaHS-assisted sulfidization with DMTD is an effective strategy for improving flotation of copper oxide–sulfide ores.

Keywords: copper oxide–sulfide ore; flotation; 2,5-Dimercapto-1,3,4-thiadiazole (DMTD); sulfidization; sodium hydrosulfide; density functional theory

Check for updates

Academic Editor: Qicheng Feng

Received: 6 July 2026
Revised: 3 August 2026
Accepted: 6 August 2026
Published: 8 August 2026

Copyright: © 2026 by the authors. Licensee MDPI, Basel, Switzerland. This article is an open access article distributed under the terms and conditions of the Creative Commons Attribution (CC BY) license.

1. Introduction

Copper is one of the most strategically important metals in modern society due to its excellent electrical and thermal conductivity, corrosion resistance, and extensive applications in power transmission, electronics, transportation, and renewable energy technologies [1–3]. Copper deposits occur mainly as oxide and sulfide ores. Approximately 20% of global copper resources are hosted in oxide and supergene sulfide minerals, while the remaining 80% are dominated by primary sulfide ores, particularly chalcopyrite and other copper-bearing

sulfide minerals. The accelerating global transition toward electrification and sustainable energy systems has substantially increased demand for copper, while the depletion of high-grade deposits has compelled the mining industry to exploit increasingly complex and low-grade resources [1,4]. Among these resources, mixed copper oxide–sulfide ores represent an important source of future copper supply. However, their efficient beneficiation remains challenging because of the markedly different surface properties and flotation behaviors of oxide and sulfide copper minerals.

Copper ore processing is a complex, multi-stage industrial operation that converts copper ores containing less than 1% Cu into 99.99% pure copper cathodes through integrated beneficiation and metallurgical processes. The recovery of copper from the resources is primarily achieved through froth flotation for sulfide ores and hydrometallurgical leaching for oxide ores [3,5]. Froth flotation is one of the most important and widely applied mineral processing techniques for sulfide ores and mixed oxide–sulfide deposits. This process is based on the differences in the physicochemical surface properties of minerals in an aqueous pulp and enables the selective recovery of complex, low-grade, and fine-grained ores (typically 20–200 μm). Froth flotation involves three phases—solid particles, liquid water, and gas bubbles—where the physicochemical characteristics of each phase strongly influence flotation performance [6–8]. Although sulfide copper minerals can generally be recovered efficiently using conventional sulfhydryl collectors, oxide copper minerals such as malachite, azurite, chrysocolla, and cuprite exhibit inherently poor floatability. This behavior is mainly attributed to the formation of hydrated surface layers and the ionic nature of surface bonding, which limit collector adsorption and prevent the development of sufficient surface hydrophobicity required for effective flotation [9–11]. Consequently, the recovery of oxide copper minerals remains a major challenge in the processing of mixed copper ores. Considerable research has therefore focused on developing effective flotation strategies for oxide copper minerals, among which sulfidization-assisted flotation has become the most widely adopted approach because of its simplicity, low cost, and industrial applicability [12–14]. In this process, reagents such as sodium sulfide (Na_2S) and sodium hydrosulfide (NaHS) generate sulfide-like active sites on mineral surfaces, thereby enhancing collector adsorption and improving flotation performance. However, the efficiency of sulfidization is highly dependent on operating conditions and reagent dosage, as excessive or insufficient sulfidization may lead to unstable surface chemistry, increased reagent consumption, and reduced flotation selectivity, limiting its industrial application [9–11]. Several studies have investigated alternative collector systems to improve the performance of conventional sulfidization-based flotation of oxide copper minerals and mixed oxide–sulfide ores. Tijsseling et al. [12] investigated a complex Cu–Co ore containing mixed oxide and sulfide minerals and demonstrated that replacing conventional xanthate with alternative thiol collectors in a controlled-potential sulfidization circuit increased copper recovery from 70% to 83%, while suggesting that hydroxamate collectors could further improve flotation performance in mixed oxide–sulfide ores. Similarly, Zare et al. [14] evaluated a low-grade complex copper ore and showed that optimized sulfidization using $(NH_4)_2S$ increased oxide copper recovery by 9.46%, whereas the addition of potassium octyl hydroxamate further improved oxide copper recovery by 6.8%. Moreover, controlled-potential sulfidization (CPS) provided an additional 10.34% increase in oxide copper recovery while reducing sulfidizer consumption compared with conventional slug sulfidization. In addition to hydroxamate-based collectors, mixed collector systems have also attracted considerable attention. Yin et al. [13] investigated the sulfidizing flotation of malachite and subsequently validated the collector system using a copper ore from the Tonglushan mine, reporting a synergistic effect between sodium butyl xanthate (NaBX) and dodecylamine (DDA), which produced higher recoveries than NaBX alone and yielded a

copper concentrate grading 15.93% with a recovery of 76.73%. Collectively, these studies demonstrate that optimizing sulfidization strategies and employing alternative or mixed collector systems can substantially enhance the flotation performance of oxide copper minerals. Nevertheless, the flotation efficiency of conventional collector systems remains highly dependent on surface chemistry and mineralogical characteristics, emphasizing the need for more efficient and selective collectors.

Recent developments in flotation reagent design have highlighted the significant potential of sulfur- and nitrogen-functionalized organic collectors for the efficient recovery of oxide copper minerals. In particular, azole- and thione-based collectors have gained increasing attention due to their strong chemical affinity toward copper-containing surface sites [15–22]. Through the formation of stable surface complexes involving Cu–S and Cu–N coordination interactions, these collectors can achieve effective adsorption on copper mineral surfaces. The resulting interfacial interactions enhance surface hydrophobicity, thereby improving mineral selectivity and flotation efficiency [20,21,23]. For instance, recent studies have demonstrated the promising performance of azole-based collectors in the flotation of oxide copper minerals. The heterocyclic azole structure provides suitable coordination environments for interaction with copper surface species, enabling selective adsorption and enhanced surface hydrophobicity. Liu et al. [19] reported that an amino-triazole-based collector exhibited improved flotation selectivity for malachite through strong interaction with copper active sites and formation of stable surface complexes. Similarly, He et al. [20] and Cheng et al. [21] showed that azole-containing collector structures contributed to enhanced flotation performance and selective separation of copper oxide minerals. These findings suggest that the molecular design of azole-based collectors offers a promising pathway for developing more selective and efficient reagents for oxide copper mineral recovery.

In addition to azole- and thione-based collectors, mercaptans are sulfur analogues of alcohols, where the oxygen atom of the hydroxyl group (R–OH) is replaced by sulfur, resulting in the general structure R–SH [24]. Recently, mercaptan-based collectors have been investigated for copper flotation applications. Nyarko et al. [25] reported that mercaptan collectors exhibited high selectivity against pyrite in the flotation of porphyry copper ore and achieved effective performance at lower dosages compared with conventional collectors such as xanthates and dithiophosphates. Furthermore, Bazmandeh and Sam [24] introduced 2,5-Dimercapto-1,3,4-thiadiazole (DMTD) as a new collector for copper sulfide ores and demonstrated its capability to improve copper recovery and flotation performance under optimized flotation conditions. In addition, recent studies have investigated DMTD as an activator in copper oxide flotation, reporting improved flotation performance of copper minerals [26,27]. However, the application of DMTD as a collector for oxide copper minerals and copper sulfide–oxide ores, particularly in complex ore systems, remains insufficiently explored. Additionally, most previous studies on advanced azole-based collectors have focused on pure mineral systems, while their performance in real copper ores containing mixed sulfide and oxide phases has received less attention. Flotation processes rely on a series of complex physicochemical interactions occurring in solid–liquid–gas multiphase systems, and these challenging situations can frequently be encountered. It is precisely at this point that Density Functional Theory (DFT) becomes a powerful method for quantitatively characterizing the exchange of matter and energy at the molecular level in these systems [28,29]. Although the flotation performance of DMTD and similar collectors has been experimentally proven, their interaction mechanisms with sulfidized mineral surfaces—and especially the role of water molecules at the solid–liquid interface during these adsorption processes—have not been fully elucidated at the molecular level. Understanding the thermodynamic driving forces that dictate the reactivity and surface adsorption of collector molecules is critical for the development of next-generation reagent

strategies. In this context, quantum chemical thermodynamic parameters obtained using Density Functional Theory (DFT) and hybrid solvation models, along with frontier molecular orbital (HOMO-LUMO) analyses, offer a powerful theoretical framework capable of explaining experimental flotation data at the atomic level. Therefore, this study aims to investigate the flotation performance of DMTD as a collector in a copper sulfide–oxide ore system and evaluate the effects of key flotation parameters on copper recovery. For this purpose, response surface methodology (RSM) is employed to systematically evaluate the flotation behavior of the DMTD collector and determine the effects and interactions of operational parameters on copper recovery.

2. Materials and Methods

2.1. Materials

Approximately 100 kg of mixed copper oxide–sulfide ore was collected from the Nasim Copper Mine, located in Bardaskan County, Razavi Khorasan Province, Iran. The bulk sample was transported to the laboratory for sample preparation and characterization prior to flotation testing. The run-of-mine ore was initially crushed in a laboratory jaw crusher to a particle size below 10 mm and subsequently reduced using a laboratory roll crusher. The crushed material was thoroughly homogenized, and representative subsamples were obtained using the conning-and-quartering method to ensure sample representativeness for subsequent analyses and flotation experiments. The representative sample was then subjected to chemical analysis by atomic absorption spectroscopy (AAS). The results indicated a total copper grade of 0.77 wt.% and an oxide copper grade of 0.4 wt.%, confirming the mixed oxide–sulfide nature of the ore. To further characterize the representative ore sample, elemental composition and mineralogical phases were determined by X-ray fluorescence (XRF) using a PHILIPS PW1410 X-ray fluorescence spectrometer (PHILIPS, Almelo, The Netherlands) and by X-ray diffraction (XRD) using a PHILIPS PW1730 X-ray diffractometer (PHILIPS, Almelo, The Netherlands) equipped with Cu Kα radiation (λ = 1.54056 Å) and operated at 40 kV and 30 mA, respectively. The elemental composition determined by XRF is summarized in Table 1, and the XRD pattern together with the identified mineral phases is presented in Figure S1. The XRD analysis identified quartz, calcite, plagioclase, and potassium feldspar as the dominant mineral phases. These findings are consistent with the XRF results, which show relatively high SiO_2 (36.70 wt.%) and CaO (17.99 wt.%), confirming that silicate and carbonate minerals constitute the major gangue components of the studied ore.

Table 1. Chemical composition of the oxide–sulfide ore sample (wt.%).

Composition	SiO_2	Al_2O_3	Fe_2O_3	CaO	MgO	Na_2O	K_2O
Content	36.70	11.61	5.38	17.99	3.61	2.53	2.79
Composition	TiO_2	MnO	P_2O_5	S	Cu	Sr	LOI *
Content	0.52	0.16	0.29	0.20	0.73	0.04	17.43

* is Loss on Ignition.

In addition, a particle size distribution analysis of the flotation feed was conducted (Figure 1), revealing a d_{80} of approximately 98 μm. This particle size was selected to closely match the typical flotation feed size used in the processing plant ($d_{80} \approx 100$ μm).

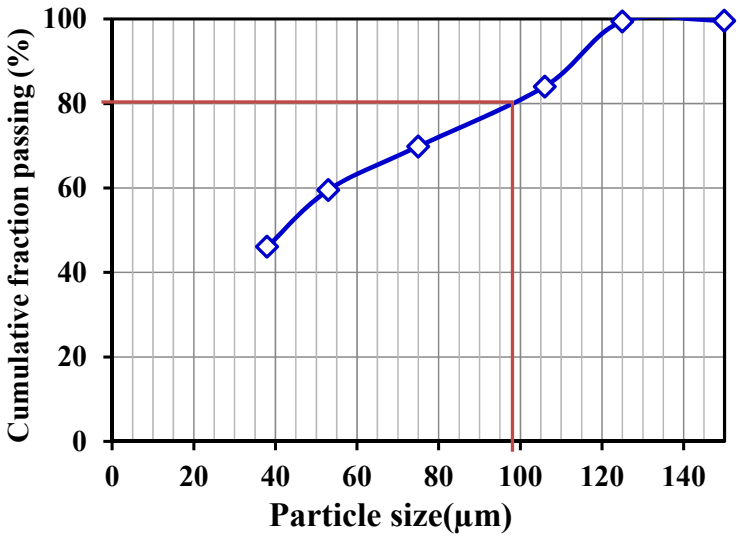


Figure 1. Particle size distribution of the studied oxide–sulfide sample.

2.2. Flotation Experiments

Flotation experiments were carried out using a laboratory-scale Denver mechanical flotation machine equipped with a 3 L flotation cell. For each test, a predetermined mass of ground ore was used according to the pulp solids concentration specified in the experimental design matrix. The sample was transferred to the flotation cell, and distilled water was added to achieve the desired pulp density. The impeller speed was maintained at 1200 rpm throughout all experiments to ensure adequate particle suspension and stable hydrodynamic conditions. The pulp pH was adjusted to the target value using lime slurry prior to reagent addition. The reagent dosages were selected within the ranges defined by the experimental design matrix. Stock solutions of sodium metasilicate (20 g/L), sodium hydrosulfide (NaHS, 20 g/L), and 2,5-dimercapto-1,3,4-thiadiazole (DMTD, 5 g/L) were prepared by dissolving the appropriate amount of each reagent in distilled water at room temperature under magnetic stirring for approximately 15 min, followed by dilution to a final volume of 1 L. The NaHS stock solution was freshly prepared prior to each set of flotation experiments, whereas MIBC was used without further dilution. Sodium metasilicate was initially added as a gangue depressant and conditioned for 2 min, followed by the addition of DMTD as the collector with a conditioning time of 4 min. Methyl isobutyl carbinol (MIBC) was subsequently added as a frother at a fixed dosage of 75 g/t and conditioned for 2 min. After completion of the conditioning stages, flotation was performed, and the froth product was collected for subsequent copper recovery analyses. The overall flotation procedure, including reagent addition sequence and conditioning stages, is illustrated in Figure S2.

The first rougher flotation stage was performed for 5 min, during which the froth concentrate was continuously collected. The pulp volume was then restored using distilled water. MIBC was subsequently added at a fixed dosage of 75 g/t, followed by 2 min conditioning, and a second rougher flotation stage was conducted for 5 min. The concentrates obtained from both rougher stages were combined as the final rougher product. Following rougher flotation, sodium hydrosulfide (NaHS) was added according to the experimental design matrix to promote the sulfidization of residual oxidized copper minerals. The pulp was conditioned for 10 min to allow sufficient interaction between the sulfidizing agent and mineral surfaces. Subsequently, DMTD was added as a scavenger collector and conditioned for 4 min, followed by the addition of MIBC at a fixed dosage of 75 g/t with 2 min conditioning. A scavenger flotation stage was then carried out for 5 min. The scavenger concentrate was collected separately, and all flotation products, including rougher concentrate,

scavenger concentrate, and tailings, were filtered, dried, and weighed prior to chemical analysis. The feed sample was also analyzed for head grade determination. Copper concentrations in all samples were determined using atomic absorption spectroscopy (AAS). Ultimately, the recovery of copper was selected as the response variable for evaluating flotation performance and optimizing the operating conditions. The recovery values were determined based on the following mass balance relationship:

$$R = \frac{Cc}{(C+T)f} \times 100 \quad (1)$$

where R is the copper recovery (%), C and T represent the dry masses of the concentrate and tailings, respectively, while f and c denote the copper grades of the feed and concentrate, respectively. The experimentally determined recovery values were subsequently utilized for model development, statistical analysis, and optimization of the flotation process.

3. Computational Setup

To reflect the activating effect of the sulfidation (NaHS) process on the malachite [30] surface at the molecular level, a localized crystal surface cluster of 40 atoms containing 8 copper (Cu) atoms was constructed. Based on the experimental observation that NaHS cannot break strong C–O bonds and reacts at weaker Cu–OH points, an active surface hydroxyl (–OH) group in the reference crystal structure was proportionally replaced with a single hydrosulfite (–SH). To maintain the electrical neutrality (charge = 0) and isoelectronic equilibrium of the cluster, a hydrogen atom was manually added to the sulfur. Electronic structure optimizations were performed using the B3LYP functional and the def2-SVP basis set in the TURBOMOLE software 7.8.1 package [31]. Def2-SVP, which strikes an optimal balance between computational cost and thermodynamic accuracy, successfully reflects the relativistic effects in the inner shells of copper atoms thanks to its Effective Nuclear Potential (ECP), while also preventing SCF convergence instabilities in multi-center transition metal systems. To capture the long-range intermolecular van der Waals interactions of the system, a D4 dispersion correction is integrated into the model; the broad electron cloud of sulfur is optimized with an m5 integration mesh and appropriate SCF damping (damp/shift) parameters. The 3D initial structures of PAX and DMTD molecules were obtained from the PubChem database (https://pubchem.ncbi.nlm.nih.gov (accessed on 5 August 2026)). The malachite surface was constructed as a cluster of 40 atoms corresponding to the stoichiometry of a unit cell, using a non-periodic model [30]. In order to prevent SCF convergence problems in multi-centered transition metal systems and to correctly optimize the large electron cloud of sulfur, the parameters scfdamp start = 0.500 step = 0.010 min = 0.010 and scforbitalshift closedshell = 0.2000 were used in addition to the m5 integration mesh.

Based on this optimized Cu–S surface model, a hybrid solvation strategy was adopted to compare the adsorption mechanism and water displacement capabilities of industrial collectors (DMTD and PAX) in flotation. To avoid thermodynamic deviations caused by implicit models, the inclusion of explicit water molecules in flotation simulations is critical to accurately reflecting water–surface interactions, ranging from weak van der Waals forces to strong chemical bonds depending on the wettability character of the mineral, and the strong hydrogen bond networks that determine the collector's retention kinetics [28,29]. Accordingly, a total of four different adsorption complexes were prepared for both collectors: one containing four explicit water molecules representing local hydrogen bonding networks at the interface, and one without explicit water molecules. All systems were optimized by encapsulating them with the COSMO implicit solvation model to reflect the macroscopic dielectric effect. To quantitatively determine thermodynamic stability, a

fragmentation approach was used, incorporating the deformation energies (E_{def}) resulting from the structural adaptation processes of the system into the equation physicochemically, and the adsorption energies (ΔE_{ads}) were calculated based on the reference energies of the isolated fragments [32,33]. This strategy prevented mathematical artifacts that could arise from complex BSSE (Basis Set Superposition Error) corrections in multi-body systems; by integrating deformation energies into the equation through natural processes, a highly accurate and realistic thermodynamic profile has been obtained. The final formula, which incorporates deformation energies naturally in the calculations and is based on the fragmentation approach, is as follows:

$$\Delta E_{ads} = E_{complex} - (E_{surface} + E_{reactive} + E_{waters}) \quad (2)$$

Here, $E_{complex}$ represents the combined optimized energy of the surface, the reactive molecule (PAX or DMTD), and four water molecules; $E_{surface}$ represents the optimized energy of only the Cu-S surface; $E_{reactive}$ represents the optimized energy of only the reactive molecule (PAX or DMTD); and E_{waters} represents the optimized energy of the cluster of four water molecules (tetramer). In addition to energetic analyses, frontier molecular orbital (HOMO–LUMO) energy gaps were evaluated to elucidate the chemical reactivity and electron exchange between the collectors and the surface, and the electronic profiles of the four models were detailed [32,34].

4. Results and Discussion

4.1. Design of Experiments

The effects of flotation operating variables on copper recovery were evaluated using response surface methodology (RSM). To this end, a central composite design (CCD) was employed to design the experiments, develop the predictive response surface model, and quantify the linear, quadratic, and interaction effects of the selected process variables. Five operational parameters, namely pulp pH, DMTD dosage, sodium silicate dosage, sodium sulfide dosage, and solids concentration, were selected as independent variables owing to their significant influence on the flotation behavior of copper oxide minerals. The experimental design consisted of 29 runs ($N = 2^{(5-1)} + 2 \times 5 + 3 = 29$), including factorial, axial, and center points, enabling the assessment of linear, quadratic, and interaction effects of the investigated variables. The three replicated center-point experiments were used to estimate the pure experimental error, evaluate the repeatability of the experimental data, and support the ANOVA. The coded and actual levels of the factors are summarized in Table 2, while the complete design matrix and corresponding flotation recovery values are presented in Table 3. The experimental recovery values were subsequently utilized to develop the predictive model, evaluate factor significance through ANOVA, and determine the optimum operating conditions using the desirability function approach.

Table 2. Experimental factors, coded levels, and actual values selected for the RSM–CCD in the flotation study of oxide–sulfide copper ore.

Factor	Symbol	Coded Levels				
		−2	−1	0	+1	+2
		Actual Level				
pH	A	7	8	9	10	11
DMTD dosage (g/t)	B	50	100	150	200	250
Sodium metasilicate dosage (g/t)	C	50	200	350	500	750
NaHS dosage (g/t)	D	0	250	500	750	1000
Solid (%)	E	15	20	25	30	35

Table 3. RSM–CCD experimental design matrix and corresponding copper recovery values obtained from flotation experiments.

Run	A	B	C	D	E	Cu Recovery (%)
1	10	100	200	250	20	45.38
2	9	150	650	500	25	59.98
3	9	150	350	500	25	58.47
4	10	200	200	750	20	55.49
5	8	100	500	250	20	44.78
6	8	200	500	750	20	59.68
7	9	150	350	500	25	59.45
8	9	150	350	500	25	57.86
9	9	250	350	500	25	59.53
10	9	150	350	1000	25	64.88
11	10	100	200	750	30	53.13
12	10	100	500	250	30	51.53
13	10	100	500	750	20	57.59
14	8	200	200	750	30	54.88
15	9	150	350	0	25	50.32
16	8	100	200	250	30	51.95
17	7	150	350	500	25	48.45
18	10	200	500	250	20	54.5
19	11	150	350	500	25	51.05
20	9	150	50	500	25	50.63
21	8	100	200	750	20	46.06
22	8	100	500	750	30	50.21
23	10	200	500	750	30	59
24	10	200	200	250	30	53.94
25	8	200	200	250	20	50.47
26	9	50	350	500	25	49.41
27	9	150	350	500	15	49.7
28	8	200	500	250	30	47.73
29	9	150	350	500	35	50.24

4.2. Statistical Modeling

The experimental recovery data were used to develop and evaluate the predictive models for copper recovery. Within RSM, the relationship between the process variables and the response can be represented by either first- or second-order polynomial models [35,36]. Given the nonlinear behavior of flotation systems and the potential interactions among operating variables, a second-order polynomial model was employed to describe the relationship between the operating variables and copper recovery. The general form of the model is presented in Equation (S1) in the Supplementary Information [35,36].

Several empirical models, including linear, two-factor interaction (2FI), quadratic, and cubic models, were evaluated to identify the most appropriate model for describing the flotation response. The model selection results are summarized in Table S1 (Supplementary Information). Based on the statistical evaluation, the quadratic model was selected because it adequately captured the nonlinear behavior and interaction effects of the operating variables, whereas the cubic model was excluded due to aliasing. The final regression equation in terms of coded variables, after removing statistically insignificant terms, is presented as Equation (S2). The corresponding ANOVA results for the selected quadratic model are summarized in Table 4.

Table 4. ANOVA results of the quadratic model developed for copper recovery.

Source	SS	DF	MS	*F*-Value	*p*-Value	
Model	680.5	13	52.35	16.9	<0.0001	Significant
A: pH	37.5	1	37.5	12.11	0.0034	
B: DMTD (g/t)	127.42	1	127.42	41.14	<0.0001	
C: Sodium metasilicate (g/t)	43.79	1	43.79	14.14	0.0019	
D: Sodium hydrosulfide (g/t)	175.39	1	175.39	56.63	<0.0001	
E: Solid (%)	3.76	1	3.76	1.21	0.2879	
AC	15.29	1	15.29	4.94	0.0421	
BE	19.36	1	19.36	6.25	0.0245	
CD	25.3	1	25.3	8.17	0.012	
CE	37.76	1	37.76	12.19	0.0033	
A^2	117.58	1	117.58	37.96	<0.0001	
B^2	23.36	1	23.36	7.54	0.015	
C^2	14.21	1	14.21	4.59	0.049	
E^2	111.58	1	111.58	36.03	<0.0001	
Residual	46.46	15	3.1			
Lack of Fit	45.17	13	3.47	5.4	0.1669	Not significant
Pure Error	1.29	2	0.64			
Cor Total	726.96	28				
Std. Dev.	1.76					
R^2	0.9361					
Adeq Precision	15.668					
PRESS	190.42					

The ANOVA results (Table 4) confirmed the significance of the quadratic model (F-value = 16.9, $p < 0.0001$), indicating its suitability for describing copper recovery behavior. Among the linear terms, NaHS dosage (D) exhibited the strongest influence on recovery, followed by DMTD dosage (B), sodium metasilicate dosage (C), and pulp pH (A).

The pronounced effect of NaHS is attributed to its role in the sulfidization of oxidized copper minerals, where HS^- species generated from NaHS react with surface copper sites to form sulfur-containing Cu–S species. The formation of these sulfide species promotes collector adsorption and enhances mineral hydrophobicity, thereby improving flotation performance [37,38]. The significant contribution of DMTD further highlights the importance of collector–mineral interactions in flotation performance. The significant interaction terms (AC, BE, CD, and CE) demonstrate that copper recovery is governed by the combined effects of operating variables rather than independent factor contributions. In particular, the interaction between NaHS and sodium metasilicate indicates the important balance between mineral sulfidization and gangue depression during oxide copper flotation. The significance of the quadratic terms (A^2, B^2, C^2, and E^2) confirms the nonlinear response of the flotation system and the existence of optimum operating regions. The model reliability was supported by the insignificant lack-of-fit (p = 0.1669), high R^2 value (0.9361), and adequate precision (15.668), confirming the applicability of the developed model within the experimental range. The relatively low standard deviation (1.76) and acceptable PRESS value (190.42) further support the predictive reliability of the model. The predictive performance of the developed quadratic model was further verified using residual diagnostic plots and by comparing the predicted and experimental copper recovery values (Figure S3). The diagnostic plots confirmed the adequacy of the model, showing an approximately normal distribution of residuals, good agreement between predicted and experimental values, and randomly distributed residuals without any systematic pattern, indicating that the model provides reliable predictions within the investigated experimental range.

4.3. Individual and Synergistic Effects of Process Parameters

Following model validation, the effects of pH, DMTD dosage, sodium metasilicate dosage, sodium hydrosulfide dosage, and solids concentration on malachite flotation recovery were evaluated using perturbation plots, one-factor response curves, contour

plots, response surfaces, and interaction analysis. The perturbation plot and one-factor response curves (Figure 2) demonstrate the relative influence of the investigated variables on copper recovery. The slope and curvature of the perturbation curves provide an indication of the sensitivity of copper recovery to changes in each variable. Among the studied parameters, NaHS dosage exhibited the highest sensitivity, which agrees with the ANOVA results identifying NaHS as the most influential linear factor. This dominant effect can be attributed to the essential role of sulfidization in activating the malachite surface, promoting the formation of sulfur-containing sites that enhance DMTD adsorption and mineral hydrophobicity. Increasing DMTD dosage resulted in a continuous improvement in recovery, reflecting the enhanced collector interaction with the activated mineral surface. Similarly, sodium metasilicate showed a positive contribution, likely due to improved pulp dispersion and reduced interference from fine particles or slime coatings. In contrast, pH and solids concentration exhibited nonlinear trends, indicating the presence of optimum operating regions. Recovery increased with increasing pH up to approximately 9–10 and then decreased, suggesting that excessive pH values may negatively affect reagent interaction and surface chemistry. Likewise, the optimum solids concentration occurred near the central range, where favorable particle dispersion and bubble–particle attachment conditions were achieved.

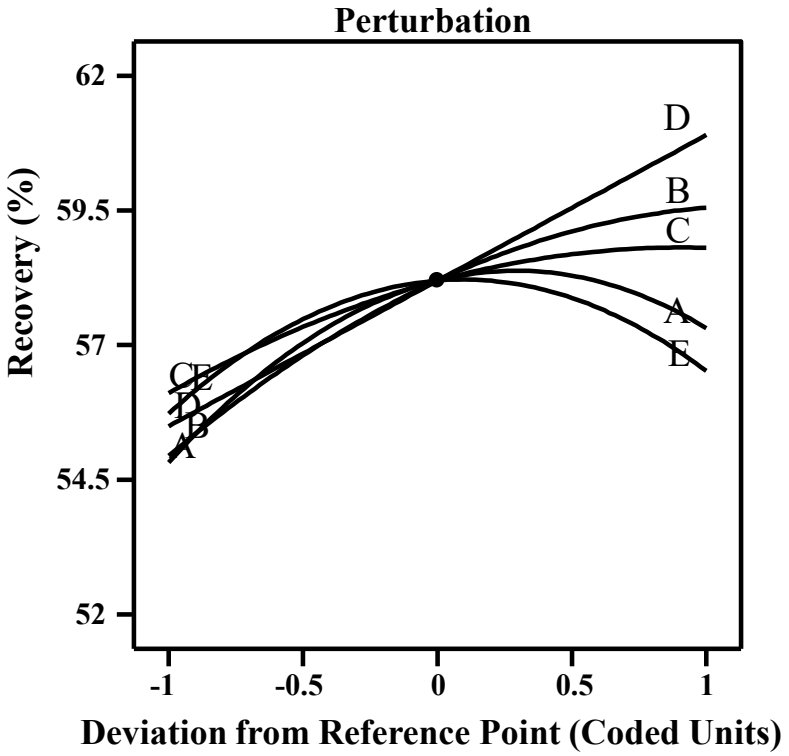


Figure 2. Perturbation plot illustrating the individual effects of pH (A), DMTD dosage (B), sodium metasilicate dosage (C), sodium hydrosulfide dosage (D), and solids concentration (E) on copper recovery.

To further explore the response behavior within the experimental domain, the combined effects of the investigated variables were analyzed using three-dimensional response surface and contour plots generated by RSM as shown in Figures 3–8. Figure 3 illustrates the combined influence of pH and DMTD dosage on copper recovery. As evident from the response surface and contour plots, copper recovery improved with increasing pH and collector dosage, reaching its highest values under moderately alkaline conditions and intermediate-to-high DMTD dosages. This trend suggests that alkaline conditions promote the formation and stabilization of sulfide species on the malachite surface, thereby enhancing DMTD adsorption and increasing surface hydrophobicity. Nevertheless, the

diminished slope of the response surface at elevated collector dosages indicates the progressive saturation of available adsorption sites, resulting in only marginal improvements in recovery beyond the optimum dosage range.

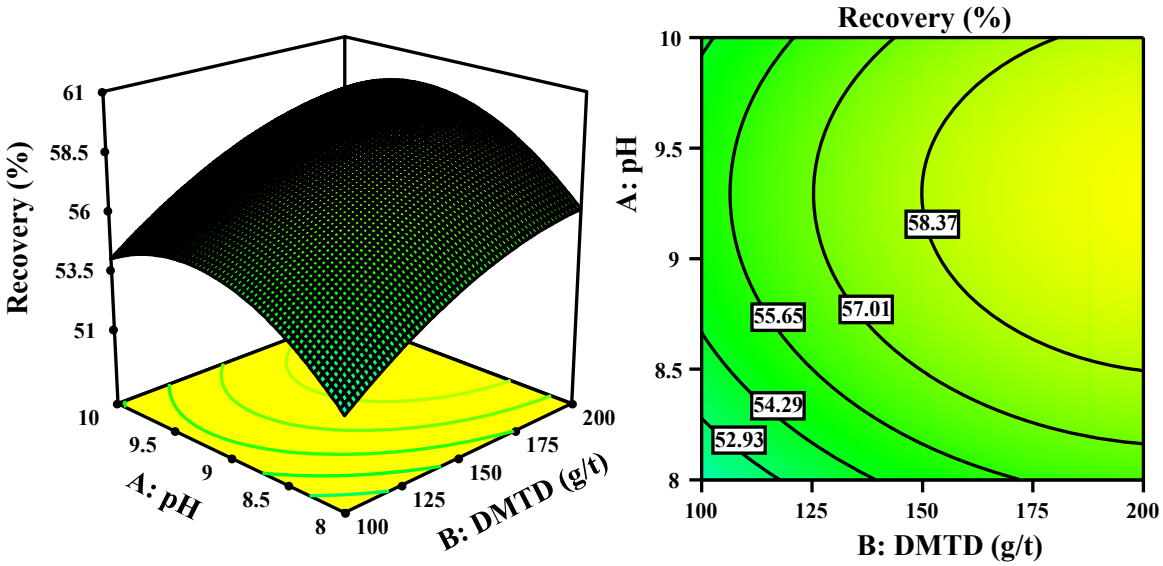


Figure 3. 3D response surface and contour plots illustrating the combined effect of pH and DMTD dosage on copper recovery.

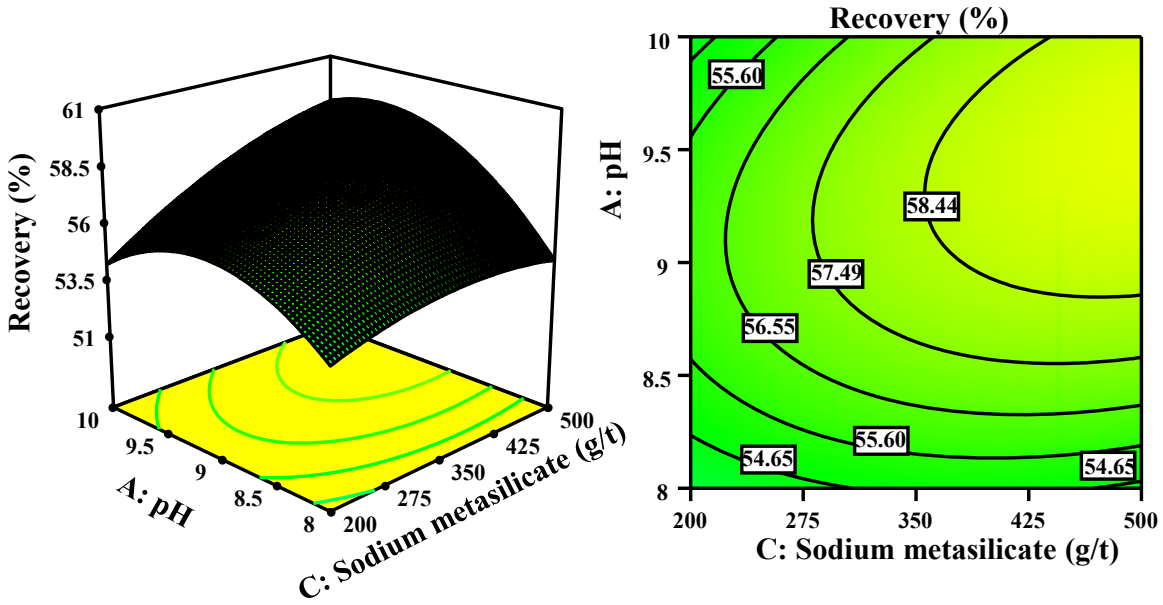


Figure 4. 3D response surface and contour plots illustrating the combined effect of pH and sodium metasilicate dosage on copper recovery.

A further refinement of the recovery response was observed through the combined adjustment of pH and sodium metasilicate dosage (Figure 4). Copper recovery increased with increasing sodium metasilicate dosage, particularly within the moderately alkaline region, with the maximum recovery achieved around pH 9.0–9.5 at relatively high dispersant levels. This trend indicates that sodium metasilicate exhibits its highest effectiveness under suitable alkaline conditions, where silicate species can effectively disperse fine particles and depress gangue minerals, thereby improving collector accessibility. However, the limited recovery improvement at excessive or unfavorable pH conditions suggests that pulp chemistry plays a critical role in controlling the overall flotation response.

Figure 5 highlights the recovery behavior as a function of DMTD dosage and pulp solid percentage. The contour and response surface plots reveal that copper recovery increases markedly with increasing collector dosage, particularly at lower pulp densities. Under these conditions, improved reagent dispersion and greater accessibility of mineral surfaces promote DMTD adsorption and enhance flotation performance. However, at higher pulp densities, intensified particle interactions and reduced reagent availability limit the effectiveness of additional collector dosage. These results demonstrate that the optimum collector performance depends strongly on maintaining a suitable balance between DMTD concentration and slurry density.

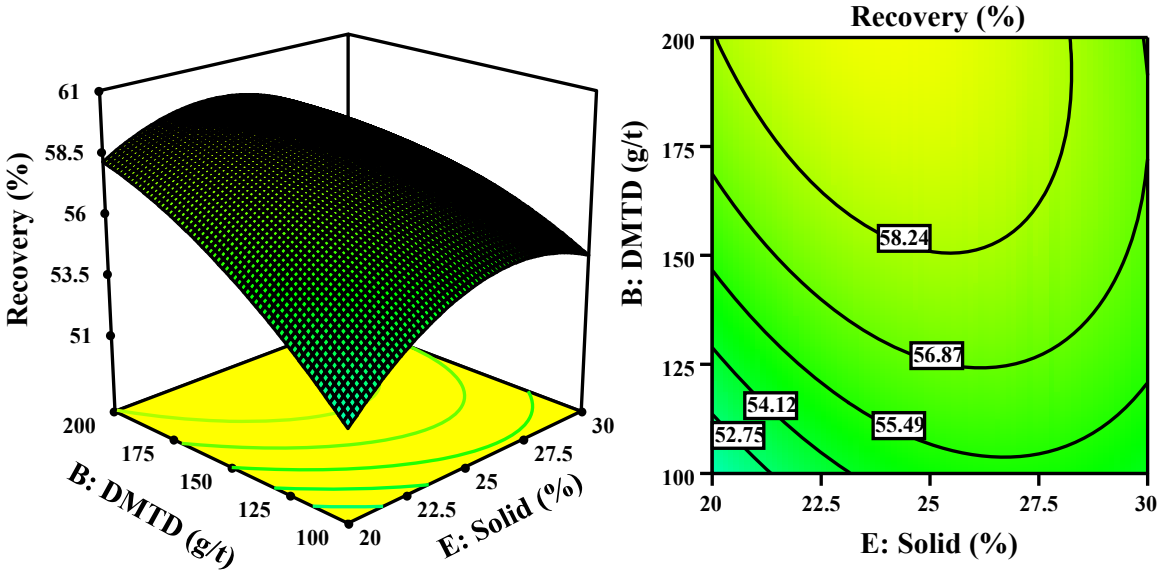


Figure 5. 3D response surface and contour plots illustrating the combined effect of DMTD dosage and pulp solid percentage on copper recovery.

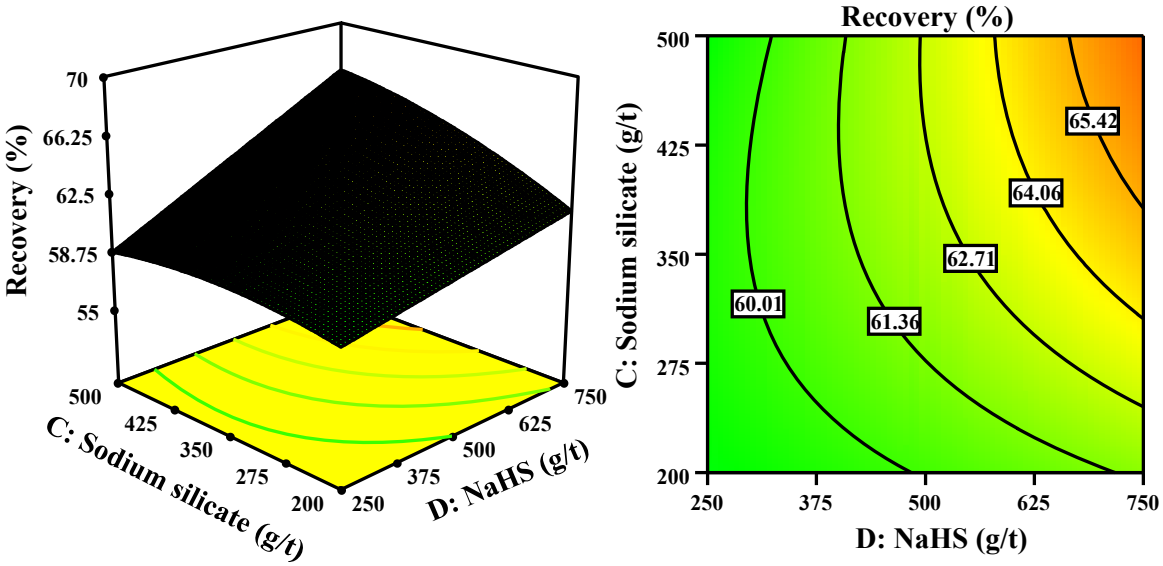


Figure 6. 3D response surface and contour plots illustrating the combined effect of sodium metasilicate and sodium hydrosulfide dosages on copper recovery.

Another notable synergistic effect was observed between sodium metasilicate and sodium hydrosulfide dosages (Figure 6). Copper recovery increased progressively with increasing concentrations of both reagents, with the highest recovery achieved at elevated NaHS dosages combined with moderate-to-high sodium metasilicate levels. This enhanced

response can be attributed to the complementary roles of these reagents, where NaHS promotes malachite surface activation through sulfidization, while sodium metasilicate improves pulp selectivity by dispersing fine particles and depressing gangue minerals. The simultaneous enhancement of surface activation and mineral selectivity facilitates collector adsorption and strengthens bubble–particle attachment, leading to improved flotation performance.

The recovery response associated with sodium metasilicate dosage and pulp solid percentage is presented in Figure 7. Copper recovery increased with increasing sodium metasilicate dosage across the studied range; however, this improvement became less pronounced at higher pulp densities. Under dilute pulp conditions, sodium metasilicate effectively disperses fine particles and minimizes slime coating, enhancing mineral selectivity and flotation performance. In contrast, increased pulp density promotes particle crowding and stronger interparticle interactions, which restrict the dispersing efficiency of sodium metasilicate. The response surface indicates that intermediate pulp densities provide a favorable balance between reagent distribution, particle suspension, and flotation kinetics.

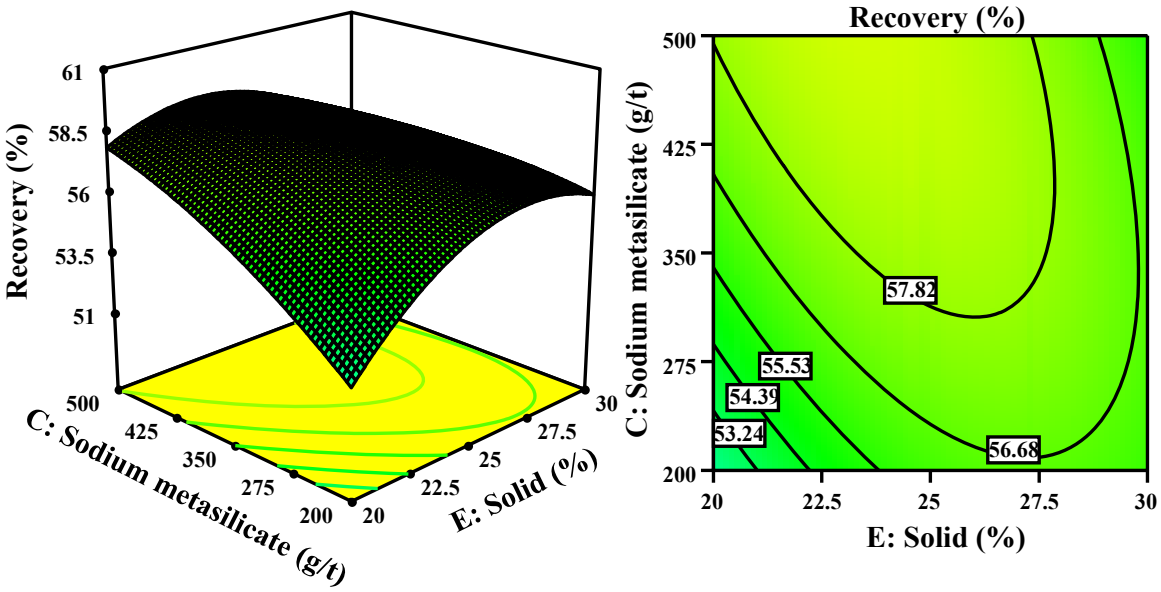


Figure 7. 3D response surface and contour plots illustrating the combined effect of sodium metasilicate dosage and pulp solid percentage on copper recovery.

Furthermore, the combined effect of NaHS and DMTD dosages on copper recovery is displayed in Figure 8. As shown in the response surface and contour plots, copper recovery gradually increased with increasing NaHS and DMTD dosages, reaching the highest values at the upper levels of both variables. This improvement can be attributed to the surface sulfidization induced by NaHS. Under alkaline flotation conditions, NaHS dissociates predominantly to produce hydrosulfide (HS^-) species, which react with exposed copper oxide surface sites to form sulfur-containing copper species or a thin copper sulfide-like layer. Consequently, the originally hydrophilic oxide surface is transformed into a sulfidized surface that is more amenable to collector adsorption [39,40]. Therefore, increasing the NaHS dosage promotes the formation of additional sulfidized surface sites, facilitating the adsorption of DMTD molecules and resulting in enhanced surface hydrophobicity and improved copper recovery.

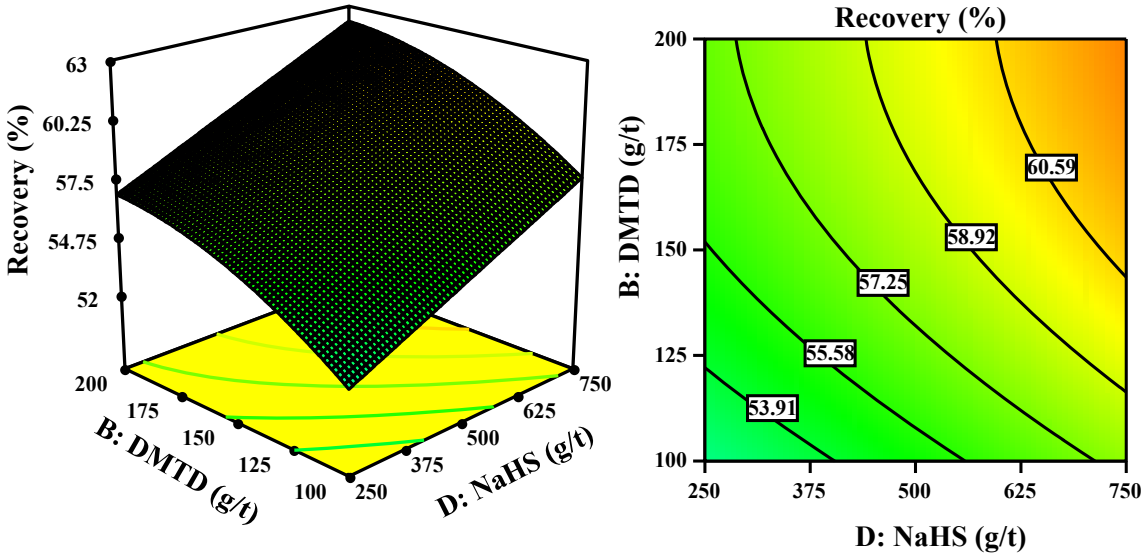


Figure 8. 3D response surface and contour plots illustrating the combined effect of DMTD and sodium hydrosulfide dosages on copper recovery.

Overall, the RSM analysis highlights that copper recovery is determined by the combined contribution of reagent chemistry and pulp conditions rather than by individual factors alone. Among the studied parameters, sodium hydrosulfide dosage showed the most significant effect, reflecting its critical role in activating the malachite surface through sulfidization. The contributions of DMTD and sodium metasilicate were mainly associated with enhanced collector adsorption and improved mineral selectivity, respectively. The significant model terms obtained from ANOVA further demonstrate the complexity of the flotation system and the importance of considering variable combinations when interpreting recovery behavior. The identified synergistic relationships provide deeper insight into the mechanisms governing malachite flotation and support the development of an optimized reagent strategy in the following section.

4.4. Process Optimization and Model Validation

Numerical optimization was performed using the desirability function approach in Design-Expert software to determine the optimum operating conditions for maximizing copper recovery. The optimum conditions predicted by the model were pH 9.40, DMTD dosage of ~199 g/t, sodium metasilicate dosage of ~491 g/t, sodium hydrosulfide dosage of ~748 g/t, and pulp solid concentration of ~24%, resulting in a predicted copper recovery of 64.91% with a desirability value of 1. The optimized conditions and the results of the confirmation flotation experiments are summarized in Table 5. Two independent validation experiments conducted under the predicted optimum conditions yielded copper recoveries of 63.79%, and 64.27%, with an average recovery of 64.03%. The close agreement between the experimental and predicted values (a difference of 0.88 percentage points and a relative error of 1.36%) confirms the accuracy and predictive capability of the developed model and demonstrates the reliability of the RSM-based optimization approach for determining effective flotation conditions.

Table 5. RSM-predicted optimum conditions and experimental validation results for optimizing copper recovery in flotation.

Parameters	pH	DMTD (g/t)	Sodium Metasilicate (g/t)	Sodium Hydrosulfide (g/t)	Solid (*w*/*w*,%)	Cu Recovery (%)
Model projections	9.4	198.84	491.34	748.26	23.92	64.91
Model validation	9.5	200	500	750	25	64.03

The optimized flotation system was further analyzed using perturbation analysis to assess the effect of individual process variables on copper recovery around the optimum operating point (Figure 9). The obtained trends indicate that sodium hydrosulfide and DMTD dosages exert the strongest influence near the optimum region, highlighting the critical role of surface activation and collector availability in governing flotation performance. Sodium metasilicate exhibits a moderate positive contribution, suggesting its supportive role in enhancing flotation conditions, whereas pulp solid percentage shows a distinct nonlinear trend, indicating the presence of an optimal operating range rather than a continuous improvement in copper recovery with increasing solids concentration. Overall, the perturbation analysis confirms that the selected operating conditions represent a balanced interaction between reagent dosages and slurry characteristics, resulting in improved copper recovery. A closer examination of the perturbation behavior shows that pulp solid percentage is the most sensitive variable around the optimum region due to its pronounced curvature, emphasizing the importance of maintaining suitable slurry density and hydrodynamic conditions. DMTD dosage also shows a strong positive response, confirming the importance of collector availability for enhancing mineral surface hydrophobicity. In contrast, the broader pH optimum region suggests that moderate pH variations have a limited effect on recovery. Accordingly, the relative sensitivity of the variables can be ranked as: Solid percentage (E) > DMTD dosage (B) > pH (A) ≈ Sodium hydrosulfide dosage (D) ≈ Sodium metasilicate dosage (C). The high desirability value (1) and close agreement between predicted and experimental recovery further confirm the reliability and robustness of the developed model.

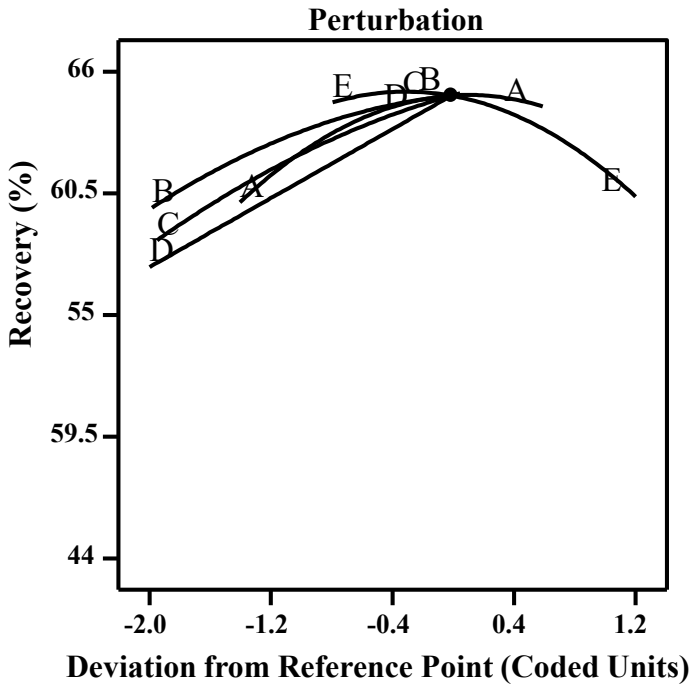


Figure 9. Perturbation plot illustrating the influence of flotation variables on copper recovery around the optimum operating point.

4.5. Performance Comparison of DMTD and PAX Under Optimized Flotation Conditions

Following the optimization stage, the flotation performance of DMTD was benchmarked against that of the plant collector (PAX) under identical operating conditions. Since all comparative experiments were conducted using the flotation parameters optimized through response surface methodology (RSM) and subsequently validated experimentally, the observed differences can be attributed primarily to collector chemistry rather than vari-

ations in process conditions. As illustrated in Figure 10, DMTD consistently outperformed PAX in both copper recovery and concentrate grade for the two samples investigated. However, the magnitude of the response was strongly dependent on the oxidation degree of the ore. For the studied ore, which contained a significantly higher proportion of oxidized copper minerals (CuOx ≈ 0.4%, corresponding to nearly 52% of the total copper), replacing PAX with DMTD increased copper recovery from 56.89% to 64.03%, corresponding to an absolute gain of 7.14 percentage points (12.6% relative increase). At the same time, the concentrate grade rose from 7.05% to 7.84%. In contrast, for the plant feed sample with a substantially lower oxidized copper content (CuOx = 0.172, CuT = 0.646), recovery increased from 67.5% to 74.2%, whereas the concentrate grade increased from 7.77% to 8.81%. Notably, the greatest increase in copper recovery was observed in the highly oxidized ore, where flotation performance is typically constrained by the limited floatability of copper oxide minerals. This behavior suggests that DMTD interacts more effectively with the sulfur-rich surface species generated during NaHS sulfidization, thereby mitigating the adverse impact of mineral oxidation on collector adsorption and particle hydrophobicity. Moreover, the simultaneous increase in both recovery and concentrate grade indicates that the improved performance was not achieved through non-selective particle collection, but rather through a more selective attachment to copper-bearing minerals. It is also important to note that the flotation conditions used for the comparative tests were optimized based on the highly oxidized ore. Despite this, DMTD maintained its superior performance not only in the ore used for optimization but also in the plant feed sample with a markedly different mineralogical composition. This finding highlights the robustness of the DMTD–NaHS system and demonstrates its ability to sustain flotation efficiency across ores with varying oxidation levels. Therefore, the advantage of DMTD extends beyond a simple increase in copper recovery; it provides a more resilient and selective flotation response in complex copper oxide–sulfide systems, making it a promising alternative to conventional xanthate-based collectors for the treatment of mixed copper ores.

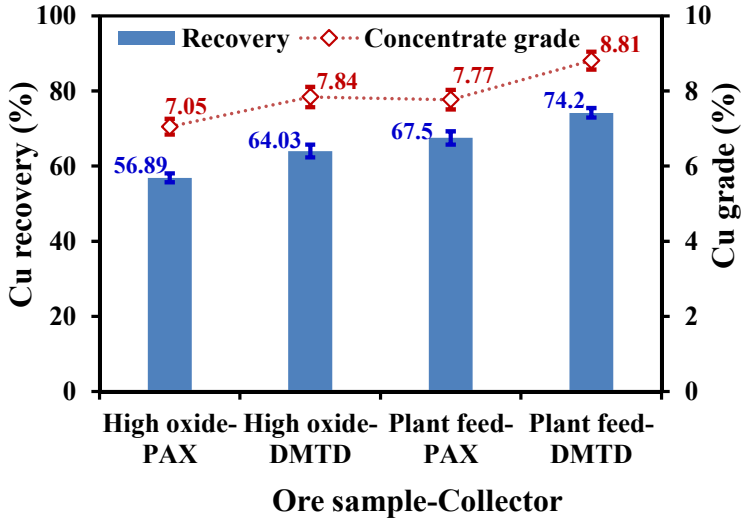


Figure 10. Comparison of copper recovery and concentrate grade obtained with DMTD and PAX for the studied ore and plant feed under optimized flotation conditions.

The superior metallurgical performance of DMTD, achieving a 64.03% copper recovery and higher concentrate grade compared to PAX, is directly confirmed by our DFT calculations. In particular, the highly exothermic adsorption energy (−6.74 eV) and the strong hydrogen bonding network established at the solid–liquid interface allow DMTD to interact more effectively with the sulfidized surface, explaining the increased macroscopic selectivity observed in Figure 10.

4.6. Flotation Kinetics Analysis

Flotation kinetics describes the rate at which particles are recovered during the flotation process and employs mathematical models to predict recovery and concentrate quality as a function of time. Understanding flotation kinetics is fundamental to the design, control, and optimization of flotation circuits, ultimately leading to improved process efficiency [39].

To evaluate the performance of the DMTD collector, rougher flotation kinetic tests were conducted using a plant feed sample under the previously established optimum operating conditions. The results obtained with DMTD were compared with those achieved using PAX, the collector currently used in the industrial flotation circuit. The corresponding results are presented in Figure 11. It should be noted that the sulfidizing agent was added during the rougher flotation stage in all kinetic experiments.

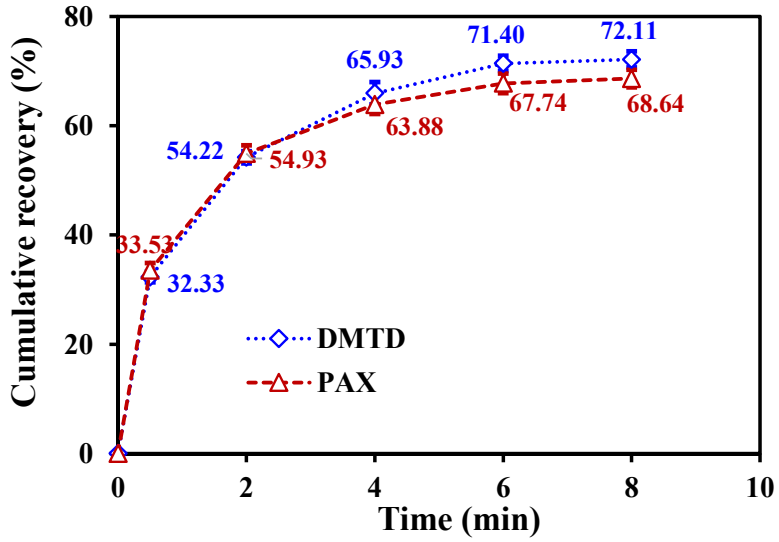


Figure 11. Cumulative recovery as a function of flotation time for DMTD and PAX during rougher flotation.

As shown in Figure 11, cumulative recovery increased with flotation time for both collectors, with a more rapid increase observed during the initial stage of flotation. DMTD consistently achieved higher cumulative recovery than PAX after 2 min of flotation. At the end of the flotation test (8 min), the cumulative recovery reached 72.11% for DMTD, compared with 68.64% for PAX. These results indicate that DMTD enhanced cumulative recovery under the optimized operating conditions. In addition, the average concentrate grade obtained with DMTD was 9.18%, compared with 8.02% for PAX, indicating that the higher recovery achieved by DMTD was accompanied by an improvement in concentrate quality. To gain further insight into the flotation behavior, the experimental data were fitted using the classical first-order kinetic model, one of the most widely used models for describing flotation kinetics. This model assumes that the flotation rate is proportional to the amount of floatable material remaining in the pulp; consequently, the recovery rate is initially high and gradually decreases with time. The mathematical expression of the first-order kinetic model is presented in Equation (3) [41,42].

$$R(t) = R_{\infty} \times (1 - e^{-kt}) \quad (3)$$

Here $R(t)$, R_{∞}, k, and t denote the recovery at time t (%), the ultimate (maximum attainable) recovery (%), the flotation rate constant (min^{-1}), and the flotation time (min), respectively.

Figure 12 demonstrates that the classical first-order kinetic model accurately described the experimental flotation behavior for both collectors, as evidenced by the close agreement between the measured and fitted recovery curves. Although PAX exhibited a slightly higher kinetic rate constant (k = 1.22 min^{-1}), indicating a faster initial flotation response, DMTD achieved a higher ultimate recovery (R_∞ = 69.51%) than PAX (R_∞ = 65.89%). The fitted curves further reveal that the difference between the two collectors became more pronounced as flotation progressed, with DMTD maintaining a continuous increase in recovery and ultimately surpassing PAX. These results suggest that, under the optimized operating conditions, DMTD improved the overall recovery potential of the flotation process despite its slightly lower flotation rate constant. This sustained increase in final recovery can be attributed to the higher electronic reactivity of DMTD in aqueous environments. As shown in DFT analysis, the significantly narrowed HOMO-LUMO energy gap (0.86 eV) of the DMTD complex facilitates superior electron transfer compared to PAX, resulting in stronger and more consistent attachment of the collector to the surface throughout the flotation process.

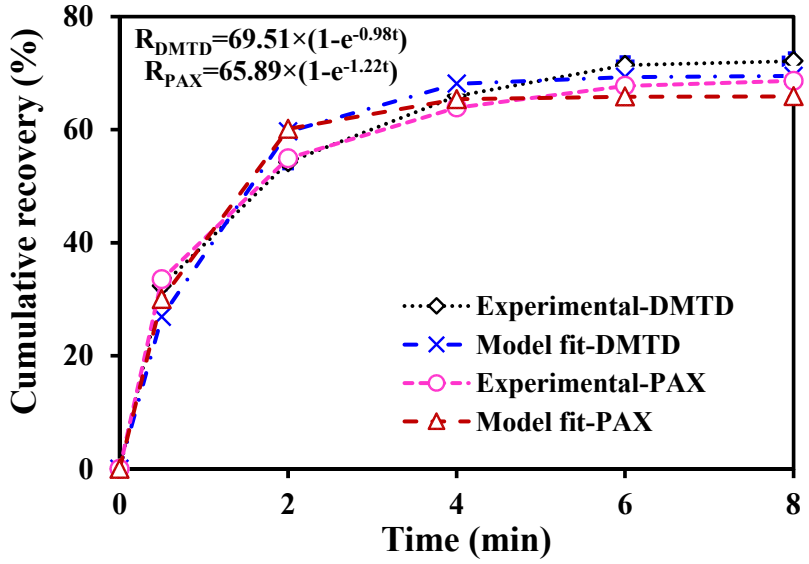


Figure 12. First-order kinetic model fitted to the rougher flotation data obtained using DMTD and PAX.

Furthermore, flotation kinetic parameters are influenced not only by the type and performance of the collector and flotation reagents, but also by the mineralogical characteristics of the ore. Because the investigated ore contained both sulfide and oxide copper minerals, the observed flotation kinetics were governed by the combined flotation behavior of these mineral phases. In general, copper sulfide minerals exhibit superior natural floatability, whereas copper oxide minerals possess highly polar and hydrophilic surfaces, requiring prior sulfidization to promote collector adsorption and flotation. Even after sulfidization, their flotation response generally remains inferior to that of sulfide minerals [9,11]. Therefore, the observed kinetic behavior, can be attributed, at least in part, to the mixed oxide–sulfide nature and overall mineralogical complexity of the flotation feed, reflecting the integrated flotation response of copper minerals with inherently different flotation behaviors.

4.7. DFT Analysis

Adsorption energies (ΔE_{ads}) and Frontier molecular orbital data (HOMO-LUMO) obtained from quantum chemical calculations clearly revealed the thermodynamic affinities of the collector molecules to the sulfidized malachite surface and their electronic reactivities

in aqueous medium (Table 6). In simulations performed only in the presence of an implicit solvent (COSMO), it was found that the DMTD molecule exhibited a stronger interaction than the conventional PAX collector (−4.70 eV), despite its single-point attachment to the surface (−4.86 eV). However, when a 4-molecule explicit water network, which reflects the nature of the solid–liquid interface much more realistically, was included in the model, the difference in thermodynamic performance between the collectors widened dramatically. The adsorption energy of PAX at the solid–liquid interface increased to −5.36 eV; The adsorption energy of DMTD reached an extremely exothermic and stable value of −6.74 eV. The main reason for this enormous increase in stabilization (−1.88 eV) observed in DMTD is the specific and strong hydrogen bond network formed by the free sulfur end, which does not react with the electronegative nitrogen atoms in the thiadiazole ring, with the water molecules at the interface. The hydrophobic alkyl chain of PAX, on the other hand, lacks this kind of secondary interfacial stabilization. In addition to thermodynamic findings, the energy gaps (ΔE_{gap}) between the Frontier molecular orbitals also confirmed this difference in reactivity at the electronic level. While the energy gaps of PAX and DMTD complexes in anhydrous medium were 1.24 eV and 1.11 eV, respectively; When the explicit water network was incorporated into the system, the energy gap of DMTD narrowed dramatically to 0.86 eV, while that of PAX remained at a relatively higher value (1.02 eV). This narrowing HOMO-LUMO gap demonstrates that the hydrogen bond network mediated by water molecules significantly facilitates electron exchange (charge transfer) between the surface and the collector. This resulting thermodynamic and electronic driving force at the molecular level explains, through a physicochemical cause-and-effect relationship, why DMTD provides much higher copper recovery and concentrate grade compared to PAX under actual flotation pulp conditions.

Table 6. Adsorption energies (ΔE_{ads}), frontier molecular orbital (HOMO and LUMO) energies, and energy gaps (ΔE_{gap}) of PAX and DMTD collectors on the sulfidized malachite surface under different solvation environments.

Collector Reagent	Solvation Model (Environment)	ΔE_{ads} (eV)	HOMO (eV)	LUMO (eV)	ΔE_{gap} (eV)
PAX	Implicit Solvent (COSMO only)	−4.70	−5.71	−4.48	1.24
PAX	Hybrid Solvent (COSMO + 4 Explicit H_2O)	−5.36	−5.34	−4.33	1.02
DMTD	Implicit Solvent (COSMO only)	−4.86	−5.66	−4.55	1.11
DMTD	Hybrid Solvent (COSMO + 4 Explicit H_2O)	−6.74	−5.45	−4.59	0.86

Note: All values were calculated at the B3LYP/def2-SVP/D4-COSMO level of theory. Adsorption energies (ΔE_{ads}) were determined using the fragmentation approach, where negative values indicate thermodynamically favorable and exothermic binding. ΔE_{gap} represents the energy separation between the HOMO and LUMO levels ($E_{LUMO} - E_{HOMO}$).

To structurally validate the obtained thermodynamic and reactivity findings, optimized adsorption geometries and Frontier molecular orbitals (HOMO-LUMO) of the complexes were analyzed via the TmoleX interface (Figure 13). During the visualization phase, boundary orbital isovalue threshold values (0.11–0.20) were deliberately kept high; thus, instead of large and scattered electron clouds, the most active core centers (reactivity nodes) where direct electron transfer occurs were isolated and highlighted. The visualizations perfectly illustrate the physical mechanism of the performance difference obtained in the thermodynamic table. Especially in scenarios containing explicit water molecules, the dashed white lines automatically generated by the algorithm based on interatomic distances clearly reveal the positional map of the hydrogen bond network (H-bond network). According to this structural map, the DMTD molecule is virtually locked to the surface by forming multiple and strong hydrogen bonds with water molecules through the nitrogen atoms in the thiadiazole ring and the free sulfur atom (Figure 13g,h). In contrast, when exposed to an aqueous environment, the PAX molecule lacked secondary active centers

capable of forming hydrogen bonds and, due to the hydrophobic repulsive force caused by its long alkyl chain, physically detached from the surface and desorbed (Figure 13c,d). Consequently, this structural evidence obtained from optimized 3D coordinates definitively proves why DMTD provides superior surface stabilization in aqueous flotation pulp in three fundamental physicochemical dimensions: thermodynamic, electronic, and geometric.

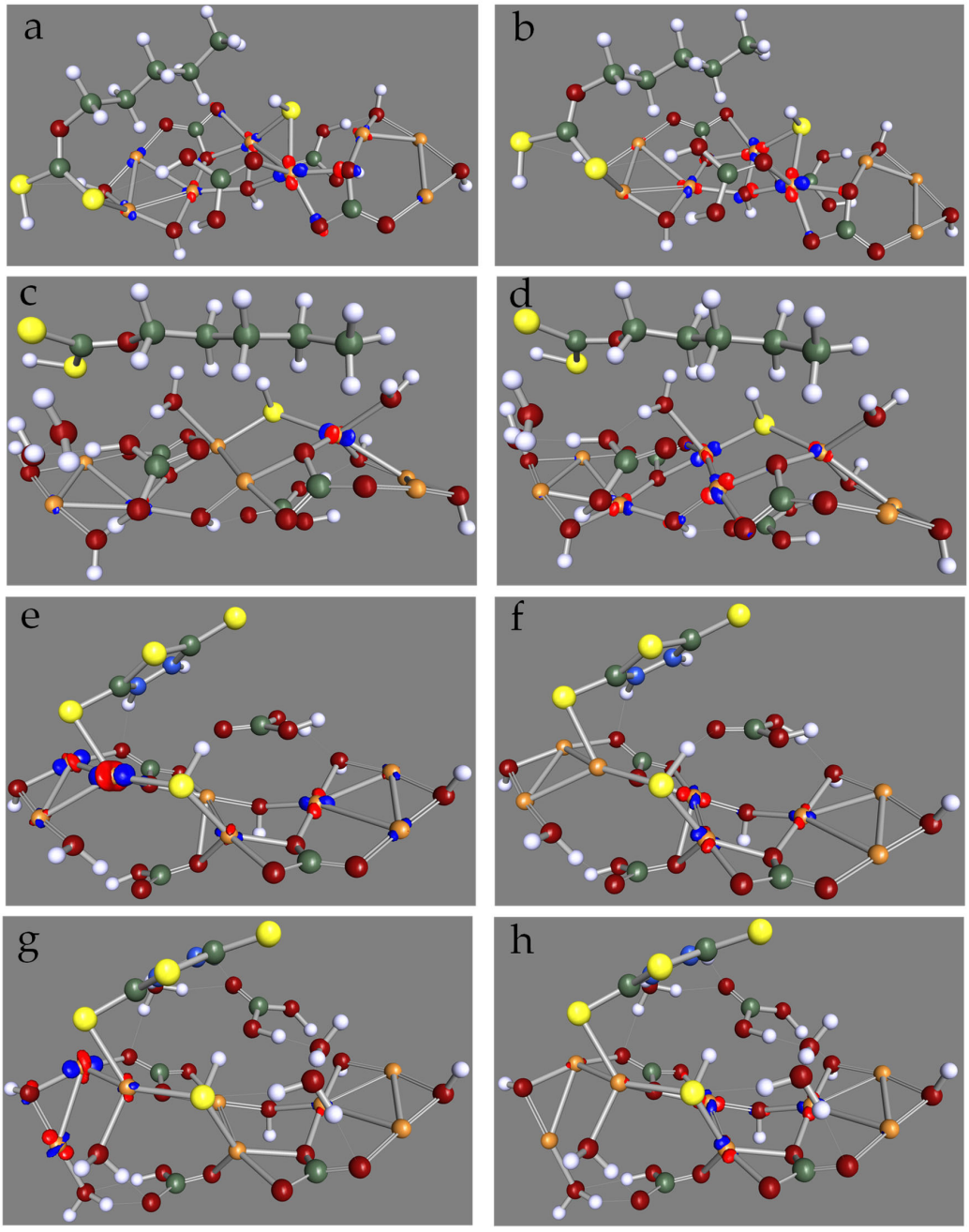


Figure 13. Optimized adsorption geometries and frontier molecular orbitals (HOMO-LUMO) of PAX and DMTD collectors interacting with a sulfidized malachite surface in different solvation environments. (**a**,**b**) PAX in anhydrous medium, (**c**,**d**) PAX in the presence of explicit water, (**e**,**f**) DMTD in anhydrous medium, and (**g**,**h**) DMTD complex in the presence of explicit water. (Left column: HOMO, Right column: LUMO. Isovalue boundary values were kept between 0.11 and 0.20 to precisely isolate the most active reactivity centers involved in electron transfer. Dashed white lines show hydrogen bonds and secondary interactions detected by the TmoleX interface based on specific interatomic distances in optimized coordinates.) Atom color legend: white (H), dark grey (C), dark red (O), yellow (S), blue (N), and orange (Cu).

5. Conclusions

This study demonstrated that the flotation of mixed copper oxide–sulfide ores can be effectively enhanced through the integration of NaHS-assisted sulfidization and DMTD-based collection. The developed RSM approach successfully described the complex behavior of the flotation system, where copper recovery was controlled by the combined effects of surface activation, collector interaction, and slurry characteristics. The quadratic model exhibited strong predictive reliability with an R^2 value of 0.9361, adequate precision of 15.67, and insignificant lack-of-fit, confirming its suitability for optimization of the investigated flotation system. The RSM-based optimization identified the optimum flotation conditions, which were experimentally implemented as pH 9.50, DMTD dosage of 200 g/t, sodium metasilicate dosage of 500 g/t, sodium hydrosulfide dosage of 750 g/t, and pulp solid concentration of 25%. Under these optimized conditions, the validation experiments achieved an average copper recovery of 64.03%, showing excellent agreement with the model prediction with a difference of 0.88 percentage points and a relative error of 1.36%. These results verify the robustness of the developed optimization framework and demonstrate that the selected reagent combination provides an effective balance between mineral surface activation, hydrophobicity development, and pulp conditions. The findings also provide valuable mechanistic insights into the flotation behavior of oxide–sulfide copper systems. NaHS plays a critical role in modifying oxidized copper mineral surfaces through sulfidization, creating more favorable sites for collector adsorption, while DMTD promotes the development of surface hydrophobicity required for efficient bubble–particle attachment. A comparative evaluation under the optimized flotation conditions further demonstrated the advantages of the DMTD-based collector system over the conventional plant collector regime. For the highly oxidized ore, copper recovery and concentrate grade increased from 56.89% and 7.05% to 64.03% and 7.84%, respectively, whereas the corresponding values for the plant feed improved from 67.50% and 7.77% to 74.20% and 8.81%. The concurrent enhancement of both metallurgical indicators demonstrates the ability of the proposed reagent scheme to sustain flotation efficiency and selectivity across ores with different oxidation characteristics. Experimental flotation findings were validated at the molecular level by Density Functional Theory (DFT) analyses involving hybrid solvation models. Quantum chemical calculations explained, through a clear physicochemical mechanism, why DMTD exhibited superior performance at the solid–liquid interface compared to PAX. DMTD achieved high thermodynamic stabilization ($\Delta E_{ads} = -6.74$ eV) by forming multiple hydrogen bonds with water molecules at the interface via reactive sites in the thiadiazole ring; PAX, on the other hand, exhibited desorption-prone behavior in the aqueous environment due to its hydrophobic alkyl chain. In addition, the HOMO-LUMO energy gap, narrowing to 0.86 eV in the DMTD complex, demonstrated that the electron transfer process mediated by water molecules significantly increased the collector reactivity. This agreement between comprehensive macroscopic optimization data and microscopic quantum mechanical evidence demonstrates that azole-based collectors are a highly reliable and strategic alternative in the enrichment of complex copper oxide–sulfide ores. The successful application of this azole-based collector in a complex copper ore system demonstrates its potential as an alternative reagent strategy for enhancing the recovery of challenging copper resources.

Supplementary Materials: The following supporting information can be downloaded at: https://www.mdpi.com/article/10.3390/min16080821/s1, Equation S1: General form of the second-order polynomial model; Equation S2. Final second-order polynomial model; Table S1. Statistical evaluation and adequacy analysis of the response surface models. Figure S1. XRD diagram of the studied oxide–sulfide sample. Figure S2. Experimental flowsheet of the rougher–scavenger flotation process,

illustrating reagent addition, conditioning, and froth collection stages. Figure S3. Diagnostic plots for evaluation of the developed quadratic model: (a) normal plot of residuals, (b) predicted against experimental values, (c) residuals versus run order, and (d) residuals against predicted values.

Author Contributions: Conceptualization, I.N. and A.A.; methodology, I.N., A.A. and H.D.; software, A.A. and D.K.; validation, I.N.; formal analysis, I.N. and A.A.; investigation, I.N., A.A., D.K. and A.H.; resources, I.N. and A.A.; data curation, I.N. and H.D.; writing—original draft preparation, I.N. and A.A.; writing—review and editing, A.A., H.D., D.K. and A.H.; visualization, I.N., A.A., D.K. and A.H.; supervision, A.A.; project administration, A.A. and A.H.; funding acquisition, A.H. All authors have read and agreed to the published version of the manuscript.

Funding: This research received no external funding.

Data Availability Statement: All data generated or analyzed during this study are presented in this manuscript. Further supporting data will be made available on request.

Acknowledgments: The authors would like to express their sincere gratitude to the Nasim Copper Mine for providing the samples and financial support for this research. The authors also gratefully acknowledge Shahrood University of Technology for providing the facilities necessary to conduct this study. Computing resources used in this work for molecular modellings were totally provided by the National Center for High Performance Computing of Turkey (UHeM) under grant number 5026352026.

Conflicts of Interest: Author Ahmad Hassanzadeh was employed by the company Maelgwyn Mineral Services Ltd. and Behraz Energy Ashkan Ltd. The remaining authors declare that the research was conducted in the absence of any commercial or financial relationships that could be construed as a potential conflict of interest.

References

1. Northey, S.; Mohr, S.; Mudd, G.M.; Weng, Z.; Giurco, D. Modelling future copper ore grade decline based on a detailed assessment of copper resources and mining. *Resour. Conserv. Recycl.* **2014**, *83*, 190–201. [CrossRef]
2. Calvo, G.; Mudd, G.; Valero, A.; Valero, A. Decreasing ore grades in global metallic mining: A theoretical issue or a global reality? *Resources* **2016**, *5*, 36. [CrossRef]
3. Jena, S.S.; Tripathy, S.K.; Mandre, N.R.; Venugopal, R.; Farrokhpay, S. Sustainable use of copper resources: Beneficiation of low-grade copper ores. *Minerals* **2022**, *12*, 545. [CrossRef]
4. Barros, K.S.; Vielmo, V.S.; Moreno, B.G.; Riveros, G.; Cifuentes, G.; Bernardes, A.M. Chemical composition data of the main stages of copper production from sulfide minerals in Chile: A review to assist circular economy studies. *Minerals* **2022**, *12*, 250. [CrossRef]
5. Davenport, W.G.; King, M.J.; Schlesinger, M.E.; Biswas, A.K. *Extractive Metallurgy of Copper*; Elsevier: Oxford, UK, 2002.
6. Bulatovic, S.M. Handbook of Flotation Reagents: Chemistry, Theory and Practice. In *Flotation of Sulfide Ores*; Elsevier: Amsterdam, The Netherlands, 2007; Volume 1.
7. Azizi, A.; Masdarian, M.; Hassanzadeh, A.; Bahri, Z.; Niedoba, T.; Surowiak, A. Parametric optimization in rougher flotation performance of a sulfidized mixed copper ore. *Minerals* **2020**, *10*, 660. [CrossRef]
8. González, D.F.; González, L.F.V. (Eds.) *Copper: From the Mineral to the Final Application*; BoD–Books on Demand: Norderstedt, Germany, 2023.
9. Feng, Q.; Yang, W.; Wen, S.; Wang, H.; Zhao, W.; Han, G. Flotation of copper oxide minerals: A review. *Int. J. Min. Sci. Technol.* **2022**, *32*, 1351–1364. [CrossRef]
10. Choi, J. A review of malachite flotation: Advanced reagents and sustainable practices. *Miner. Eng.* **2025**, *228*, 109317. [CrossRef]
11. Wei, X.; Sun, Y.; Wei, X.; Gao, P. Sulfidation reconstruction methods for improving the floatability of copper oxide minerals: A review. *Miner. Eng.* **2026**, *235*, 109843. [CrossRef]
12. Tijsseling, L.T.; Dehaine, Q.; Rollinson, G.K.; Glass, H.J. Flotation of mixed oxide sulphide copper-cobalt minerals using xanthate, dithiophosphate, thiocarbamate and blended collectors. *Miner. Eng.* **2019**, *138*, 246–256. [CrossRef]
13. Yin, W.Z.; Sun, Q.Y.; Dong, L.; Yuan, T.; Fu, Y.F.; Jin, Y.A.O. Mechanism and application on sulphidizing flotation of copper oxide with combined collectors. *Trans. Nonferrous Met. Soc. China* **2019**, *29*, 178–185. [CrossRef]
14. Zare, A.; Azizi, A.; Karamoozian, M. An investigation into the recovery of oxide copper from a complex copper ore using sulphidisation technique and hydroxamate and potassium amyl xanthate collectors. *Geosyst. Eng.* **2020**, *23*, 43–50. [CrossRef]

15. Yang, X.; Huang, Y.; Liu, G.; Liu, J.; Ma, L.; Niu, X.; Qu, X. A DFT prediction on the chemical reactivity of novel azolethione derivatives as chelating agents: Implications for copper minerals flotation and copper corrosion inhibition. *J. Taiwan Inst. Chem. Eng.* **2018**, *93*, 109–123. [CrossRef]
16. Huang, Y.; Liu, G.; Liu, J.; Yang, X.; Zhang, Z. Thiadiazole-thione surfactants: Preparation, flotation performance and adsorption mechanism to malachite. *J. Ind. Eng. Chem.* **2018**, *67*, 99–108. [CrossRef]
17. Huang, Y.; Niu, X.; Liu, G.; Liu, J. Novel chelating surfactant 5-heptyl-1,2,4-triazole-3-thione: Its synthesis and flotation separation of malachite against quartz and calcite. *Miner. Eng.* **2019**, *131*, 342–352. [CrossRef]
18. Liu, J.; Liu, G.; Huang, Y.; Zhang, Z. Tetrazinan-thione collectors for copper oxide mineral: Synthesis and flotation mechanism. *Appl. Surf. Sci.* **2019**, *491*, 624–632. [CrossRef]
19. Liu, J.; Hu, Z.; Liu, G.; Huang, Y.; Zhang, Z. Selective flotation of copper oxide minerals with a novel amino-triazole-thione surfactant: A comparison to hydroxamic acid collector. *Miner. Process. Extr. Metall. Rev.* **2020**, *41*, 96–106. [CrossRef]
20. He, S.; Wang, C.; Cheng, Z.; Li, X.; Si, Z.; Huang, Y.; Chen, L.; Zhang, Y. Synthesis and application of dithiocarbamate oxadiazole thione for flotation separation of malachite from quartz and calcite. *Adv. Powder Technol.* **2024**, *35*, 104315. [CrossRef]
21. Cheng, Z.; Wang, C.; Miao, D.; Ni, H.; Huang, Y.; Wang, M.; Chen, L.; Zhang, Y. The selective flotation behavior and mechanism of malachite with a double coordination structure amino-triazole-thione collector. *Colloids Surf. A Physicochem. Eng. Asp.* **2025**, *726*, 137979. [CrossRef]
22. Wang, H.; Shen, P.; Liu, D.; Xie, Z.; Tang, G.; Cai, J. Enhanced flotation of malachite by a benzotriazole–sodium sulfide synergistic activation system: Performance and interfacial mechanism. *J. Environ. Chem. Eng.* **2026**, *14*, 123704. [CrossRef]
23. Zhang, Z.; Wang, Y.; Liu, G.; Liu, S.; Liu, J.; Yang, X. Separation of chalcopyrite from galena with 3-amyl-4-amino-1,2,4-triazole-5-thione collector: Flotation behavior and mechanism. *J. Ind. Eng. Chem.* **2020**, *92*, 210–217. [CrossRef]
24. Bazmandeh, M.; Sam, A. Improvement of copper sulfide flotation using a new collector in an optimized addition scheme. *Physicochem. Probl. Miner. Process.* **2021**, *57*, 71–79. [CrossRef]
25. Nyarko, D.; Zanin, M.; Tsatouhas, G.; Seaman, D.; Skinner, W.; Abaka-Wood, G.; Asamoah, R. Flotation of a coarsely ground porphyry copper ore: Insights into collector efficiency. *Powder Technol.* **2025**, *470*, 121986. [CrossRef]
26. Yu, X.; Yin, Z.; Chen, Y.; Shen, P.; Wang, H.; Mao, Y.; Liu, D. Experimental and DFT study of modified malachite with 2,5-dimercapto-1,3,4-thiadiazole and its response to sulfidization-xanthate behavior. *Colloids Surf. A Physicochem. Eng. Asp.* **2024**, *693*, 134057. [CrossRef]
27. Wang, H.; Xie, Z.; Peng, R.; Xiang, Y.; Cai, J.; Shen, P.; Liu, D. Evolution and regulatory mechanism of 2,5-dimercapto-1,3,4-thiadiazole activation products on azurite: Experimental and theoretical studies. *Colloids Surf. A Physicochem. Eng. Asp.* **2024**, *702*, 135038. [CrossRef]
28. Cui, W.; Chen, J. Insight into mineral flotation fundamentals through the DFT method. *Int. J. Min. Sci. Technol.* **2021**, *31*, 983–994. [CrossRef]
29. Alizadeh Sahraei, A.; Azizi, D.; Mokarizadeh, A.H.; Boffito, D.C.; Larachi, F. Emerging Trends of Computational Chemistry and Molecular Modeling in Froth Flotation: A Review. *ACS Eng. Au* **2023**, *3*, 128–164. [CrossRef] [PubMed]
30. Süsse, P. Verfeinerung der Kristallstruktur des Malachits, $Cu_2(OH)_2CO_3$. *Acta Crystallogr.* **1967**, *22*, 146–151. [CrossRef]
31. Balasubramani, S.G.; Chen, G.P.; Coriani, S.; Diedenhofen, M.; Frank, M.S.; Franzke, Y.J.; Furche, F.; Grotjahn, R.; Harding, M.E.; Hattig, C.; et al. TURBOMOLE: Modular program suite for ab initio quantum-chemical and condensed-matter simulations. *J. Chem. Phys.* **2020**, *152*, 184107. [CrossRef] [PubMed]
32. Sarvaramini, A.; Larachi, F. Understanding the interactions of thiophosphorus collectors with chalcopyrite through DFT simulation. *Comput. Mater. Sci.* **2017**, *132*, 137–145. [CrossRef]
33. Brabson, L.M.; Medford, A.J.; Sholl, D.S. Comparing Classical and Machine Learning Force Fields for Modeling Deformation of Metal-Organic Frameworks Relevant for Direct Air Capture. *J. Phys. Chem. C Nanomater. Interfaces* **2025**, *129*, 16811–16825. [CrossRef] [PubMed]
34. Taheri, B.; Rezaei, F.; Shadjou, N.; Hassanzadeh, A. A molecular analysis on nitrile-based collectors and their application to chalcopyrite flotation. *Miner. Eng.* **2022**, *186*, 107763. [CrossRef]
35. Bezerra, M.A.; Santelli, R.E.; Oliveira, E.P.; Villar, L.S.; Escaleira, L.A. Response surface methodology (RSM) as a tool for optimization in analytical chemistry. *Talanta* **2008**, *76*, 965–977. [CrossRef] [PubMed]
36. Sepulveda, F.D.; Cortes, L.A.; Arancibia-Bravo, M.P.; Delgado, J.; Lucay, F.A.; Chacana, C.; Galleguillos, F.; Castellon, C. Optimizing flotation circuits: A comprehensive approach using design of experiments and stochastic simulation in cycle test validation. *Miner. Eng.* **2024**, *219*, 108978. [CrossRef]
37. Matsuoka, H.; Mitsuhashi, K.; Kawata, M.; Kato, T.; Tokoro, C.; Haga, K.; Shibayama, A. Surface properties of copper-sulfide minerals with sodium-hydrosulfide activation. *Miner. Eng.* **2020**, *156*, 106530. [CrossRef]
38. Moimane, T.; Peng, Y. Sulphidisation of oxides and oxidised sulphides and adsorption of thiol collectors on the sulphidised products—A critical review. *Adv. Colloid Interface Sci.* **2022**, *305*, 102697. [CrossRef] [PubMed]

39. Bulatovic, S.M. Flotation of oxide copper and copper cobalt ores. In *Handbook of Flotation Reagents: Chemistry, Theory and Practice, Volume 2—Flotation of Gold, PGM and Oxide Minerals*; Elsevier: Amsterdam, The Netherlands, 2010; pp. 47–65. [CrossRef]
40. Sobouti, A.; Rezai, B. Optimization of copper recovery from oxide-sulfide ores through gravity separation and flotation techniques. *Sci. Rep.* **2026**, *16*, 11970. [CrossRef] [PubMed]
41. Azizi, A.; Hassanzadeh, A.; Fadaei, B. Investigating the first-order flotation kinetics models for Sarcheshmeh copper sulfide ore. *Int. J. Min. Sci. Technol.* **2015**, *25*, 849–854. [CrossRef]
42. Gharai, M.; Venugopal, R. Modeling of flotation process—An overview of different approaches. *Miner. Process. Extr. Metall. Rev.* **2016**, *37*, 120–133. [CrossRef]

Disclaimer/Publisher's Note: The statements, opinions and data contained in all publications are solely those of the individual author(s) and contributor(s) and not of MDPI and/or the editor(s). MDPI and/or the editor(s) disclaim responsibility for any injury to people or property resulting from any ideas, methods, instructions or products referred to in the content.